Journal of Nanobiotechnology

RESEARCH

Open Access

Spermine delivered by ZIF90 nanoparticles alleviates atherosclerosis by targeted inhibition of macrophage ferroptosis in plaque

Yuwu Chen[1,2†], Biyi Xu[1,2†], Quan Lin[3†], Xinxin Zhu[1,2], Ying Lv[1,2], Xiaoxuan Bai[1,2], Xiuzhu Weng[1,2], Jie Du[1,2], Man Li[1,2], Yuxiao Zhu[1,2], Junke Mou[1,2], Mengyang Wang[1,2], Yuehong Wang[1,2,4*], Xing Luo[1,2,4*] and Changqing Xu[4]

Abstract

Background Nowadays, emerging evidence have suggested that the ferroptosis of macrophages could contribute to the progression of atherosclerosis (AS). Meanwhile, Spermine (Sp) could serve as an endogenous small molecule exhibiting a wide range of cardiovascular protective effects.

Methods Zeolitic imidazolate framework-90 (ZIF90) nanoparticles were synthesized and utilized to create a novel delivery nanosystem encapsulated with Sp (CD16/32-ZIF90@Sp). The efficacy of CD16/32-ZIF90@Sp in protecting against AS and ferroptosis was evaluated in ApoE$^{-/-}$ mice and macrophages, with a focus on assessing potential adverse effects in vivo.

Results CD16/32-ZIF90@Sp exhibited reliable and stable delivery of Sp within acidic environments and ATP sensitivity. CD16/32-ZIF90@Sp effectively reduced the cytotoxicity of Sp. As is evidenced by in vitro *and vivo* experiments, CD16/32-ZIF90@Sp showed precise targeting of macrophages within atherosclerotic plaques and ox-LDL-activated macrophages. Furthermore, treatment with CD16/32-ZIF90@Sp effectively attenuated the progression of AS and the ferroptosis of macrophage within plaque in ApoE$^{-/-}$ mice without causing significant side effects. Mechanistically, we found that CD16/32-ZIF90@Sp inhibited ferroptosis via improving mitochondrial function and upregulating the expression level of GPX4/xCT.

Conclusion Our study demonstrated that CD16/32-modified ZIF90 nanoparticles could effectively target macrophages within atherosclerotic plaques, leading to the inhibition of atherosclerotic plaque progression in ApoE$^{-/-}$ mice. These effects were attributed to the enhancement of mitochondrial function and the inhibition of macrophage ferroptosis, with limited side effects.

Keywords Atherosclerosis, Ferroptosis, Nanoparticles, Macrophage

†Yuwu Chen, Biyi Xu and Quan Lin contributed equally to the work.

*Correspondence:
Yuehong Wang
wangyh0327@126.com
Xing Luo
luoxing321@163.com
Full list of author information is available at the end of the article

Graphical Abstract

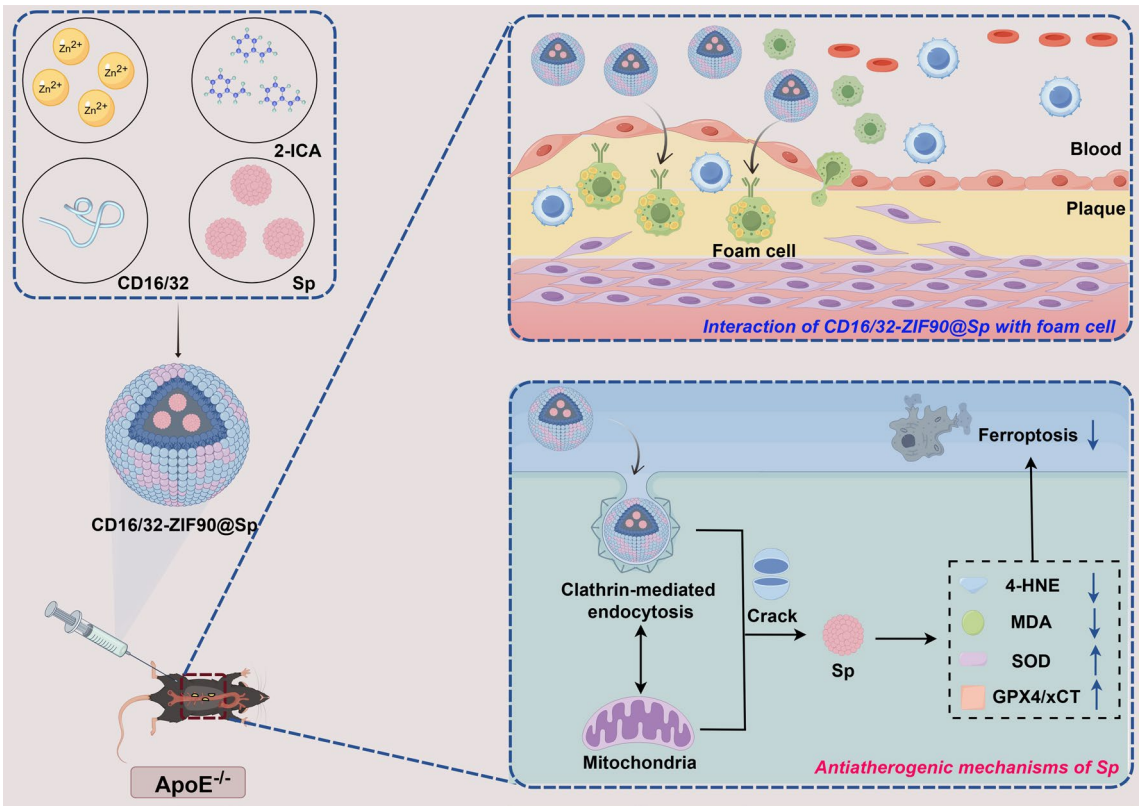

Introduction

Atherosclerosis (AS) is the pathological mechanism of the ischemic diseases, such as acute myocardial infarction, stroke and lower limb ischemia, which lead to the cardiovascular deaths and complications [1]. Nowadays, although lipid-lowering and anti-inflammatory therapy is currently considered as the first-line treatment for AS [2], there are still a large proportion of patients who have been well-treated experiencing acute ischemic events. Hence, it is essential to explore novel potential therapeutic tools for the treatment of AS [3].

AS is considered as a chronic inflammatory disease of the blood vessels, and macrophages are the main inflammatory celltype within atherosclerotic plaques. During the initial phases of AS, circulating monocytes migrate towards the vessel wall in response to chemokines, where they could differentiate into macrophages and aid in the clearance of lipids from the walls of blood vessels. Nevertheless, as the plaque progresses to advanced phases, macrophages phagocytosis within the plaque will be attenuated, and macrophages apoptosis will occur within atherosclerotic plaque [4, 5]. This phenomenon results in a heightened localized inflammation, enlargement of the necrotic core and increased plaque instability. CD16/32 is a marker that is selectively expressed by macrophages following stimulation by low density lipoprotein (LDL). This subset of cells with expression of CD16/32 exhibits a tendency towards apoptosis, pro-inflammatory reaction, and impaired phagocytic dysfunction. Also, there are increasing evidence demonstrating that the inhibition of CD16/32-positive macrophage death in plaque could serve as a potential therapeutic target for preventing the progression of AS [6, 7].

Ferroptosis is a newly discovered form of programmed cell death, whose central mechanism is cell membrane lipid peroxidation [8]. Specifically, this type of nonapoptotic regulated cell death is caused by the inhibition of anti-oxidant systems, particularly the low expression of cystine/glutamate antiporter system xc-(xCT) and glutathione peroxidase 4 (GPX4) [9]. Additionally, previous studies have reported that as the atherosclerotic plaques progressed, the expression levels of GPX4 and xCT within atherosclerotic plaques would gradually decrease, and massive ferroptotic macrophages could be observed

within the atherosclerotic plaques [10]. Mitochondrial dysfunction is acknowledged as a significant mechanism contributing to ferroptosis. The mitochondria of cells undergoing ferroptosis display reduced membrane potential, thickened mitochondrial ridges, and impaired respiratory function. Furthermore, our group and others have proved that the inhibition of ferroptosis via improving mitochondrial function could inhibit atherosclerotic progression effectively [11].

Spermine (Sp), a small endogenous polyamine, is a natural product of cellular arginine metabolism found in all eukaryotic cells [12]. Previous studies have demonstrated that Sp exerted significant cardiovascular protective effects in animal models, including AS, diabetic cardiomyopathy and ischemia–reperfusion [13, 14]. However, no significant clinical benefit of Sp has been observed. Large-dose treatment of Sp in animal experiments was hardly translated into clinical trials, which may explain the dilemma that the protective effects against myocardial injury in animals have been challenged by clinical trials [15, 16]. In addition, the excessive administration of Sp could disrupt arginine metabolism, potentially contributing to the development of metabolic disorders [17]. As such, it is imperative to refine the methods of delivery and dosage in order to enhance therapeutic outcomes while minimizing the negative impacts of Sp during the treatment of atherosclerotic cardiovascular conditions.

In recent years, there has been a growing focus on the utilization of nanoparticles as carriers for drug deliveries in the treatment of cardiovascular diseases [18, 19]. Nanoparticles are commonly employed for their abilities to facilitate targeted and sustained drug release due to their diminutive size, expansive surface area, and customizable properties [19]. Also, several studies have demonstrated that nanocarriers designed to target reactive oxygen species within atherosclerotic plaques exhibited potential anti-atherosclerotic effects with minimal adverse reactions [20, 21]. Among of them, Zeolitic Imidazolate Frameworks-90 (ZIF90) represents a subclass of metal–organic frameworks which could be produced through a self-assembly synthesis involving zinc ions and imidazole-2-carboxaldehyde (2-ICA) [22]. Due to the higher affinity of zinc ions for ATP compared with 2-ICA, ZIF90 undergoes degradation in the presence of ATP, which facilitates the release of drug. Given that mitochondria serves as the main sites for ATP production, ZIF90 is utilized for targeting drug delivery to these organelles [23, 24]. Nevertheless, there is a lack of researches examining the efficacy and safety of ZIF90-mediated drug delivery in the treatment of AS.

On the basis of the above consideration, in the present study, we utilized CD16/32 antibody-modified ZIF90 as a drug carrier for targeting delivery of Sp to macrophages within atherosclerotic plaques. Utilizing the ability of ZIF90 to target and recognize mitochondria, we investigated the effects and specific mechanisms of Sp in improving mitochondrial function and consequently suppressing ferroptosis in macrophages.

Methods

Regents

THP-1 cells were obtained from ATCC (Virginia, USA). Cell Counting Kit (CCK-8), Hoechst-PI staining assay and LDH assay were purchased from Beyotime Biotechnology (Shanghai, China). ox-LDL was purchased from Yiyuan Biotechnology (Guangzhou, China). SYBR Green and Reverse Transcription kit for PCR were purchased from Vazyme Biotech Co.,Ltd (Nanjing, China). Primary antibody sources were listed: antibodies against GPX4 (ab125066), Tomm20 (ab186735), β-actin (ab8226) and xCT (ab307601) were purchased from Abcam (Cambridge, UK). Sp was obtained from Solarbio (Beijing, China).

Synthesis and characterization of ZIF90

The details were shown in supplemental material 1.

Animals

The study was conducted according to the guidelines of the Declaration of Helsinki and approved by the institutional research ethics committee of the Second Affiliated Hospital of Harbin Medical University (YJSDW2023-031). The 6–8 weeks male ApoE$^{-/-}$ mice were divided into five groups. Normal diet (ND): The mice were fed with normal diet. High fat diet (HD): The mice were fed with western diet [25]. CD16/32-ZIF90 group: The mice were fed with western diet supplemented with equal CD16/32-ZIF90 via intraperitoneal injection. Sp group: The mice were fed with western diet supplemented with 2.5 mg/kg/day Sp via intraperitoneal injection. CD16/32-ZIF90@Sp group: The mice were fed with western diet supplemented with CD16/32-ZIF90@Sp (delivery 2.5 mg/kg Sp, 2.68 mg/kg CD16/32-ZIF90@Sp) via intraperitoneal injection. After 16 weeks, all animals were anesthetized with an intraperitoneal injection of sodium pentobarbital (50 mg/kg body weight) and then euthanized by cervical dislocation. All animal experiments were performed in accordance with National Institutes of Health guide for the care and use of laboratory animals.

Cell culture

According to previous study [26], THP-1 cells were sed in 6-well plate, 50 nM PMA was incubated for 48 h to induce into macrophages, then treated with 100 μg/ml of ox-LDL for 48 h. And different concertation Nanoparticles (NPs) were added into the medium.

CCK-8 assay and Cytotoxicity Assessment by Lactate Dehydrogenase (LDH) Assay

Cell survival was assessed via using CCK-8 (Dojindo, Japanese) and LDH assays (Jiancheng, Nanjing, China). THP-1-derived macrophages were seeded in a 96-well plate at a density of 2×10^4 cells per well and treated with ox-LDL, CD16/CD32-ZIF90, Sp, CD16/CD32-ZIF90@Sp for different time horizons. Subsequently, the cells was filled with the CCK-8 reagent (10 μL of CCK-8 working solution diluted in 100 μL of 1640 medium), which is followed by further incubation at 37 °C. Viability of cells was determined by measuring the absorbance at 460 nm via operating a microplate reader. In view of manufacturer instructions, an LDH assay kit was used to quantify LDH release.

PI/Hoechst 33,342 staining

Staining with PI/Hoechst 33,342 was performed in view of manufacturer's instructions. A 30-min treatment at 4 °C with 5ug/ml Hoechst 33,342 and 2ug/ml PI were performed on THP-1-derived macrophages, which were plated at a density of 5×10^3 cells per well. Subsequently, under a fluorescence microscope (OLYMPUS, Japan), stained cells were examined in random fields to quantify the apoptotic population.

Immunofluorescence staining

Immunofluorescence analysis was conducted on THP-1-derived macrophages and paraffin-embedded tissue sections.

As for the former, the cold acetone was applied in the fixation of macrophages, which was subsequently washed by PBS for three times (5 min). PBS containing 0.3% Triton×100 was operated to destroy the membrane of cells for 15 min, and PBS containing 5% BSA was used for blocking for 1 h. Incubation was conducted at 4 °C with primary antibodies diluted 1:100 in PBS overnight, and incubation with a secondary antibody lasting 1 h. The nucleus was dyed with DAPI for 5 min. Fluorescence microscopy was used to image the aortic root tissues (Leica, Wetzlar, Germany).

As for the later, the slides were deparaffinized via using xylene three times for 10 min each. Subsequently, the sections were rehydrated in a series of ethanol concentrations (100%, 90%, 70%) and watered for 5 min each. Slides were incubated in boiling citrate buffer (pH 6.0) for 30 min to retrieve antigens. PBS was utilized as a wash buffer. Following blocking with PBS containing 5% BSA for 1 h at room temperature, the tissues were exposed to primary antibodies which were diluted 1:100 in PBS and stored overnight at 4 °C. Following the initial step, a 1-h incubation with a secondary antibody was conducted. Subsequently, the tissues were counterstained with DAPI for DNA visualization. Fluorescence microscopy was used to image the aortic root tissues (Leica, Wetzlar, Germany).

The analysis of Western Blot

The Western blot procedure was conducted in accordance with previously published methods [27]. Specifically, the samples were homogenized in RIPA (Beyotime Biotechnology, Shanghai, China) with 1 mM PMSF (Beyotime Biotechnology, Shanghai, China) for 1 h, whose protein lysates were sonicated for 2 min, and were followed by centrifugation at 12,000 g for 15 min at 4 °C. We then loaded the same amounts of protein on a SDS-PAGE gel, electrophoresed it, and transferred it to the PVDF membranes. Blocking grade milk 5% was used to block the membranes for 1 h at least, followed by overnight incubation with specific primary antibodies. After three washings with TBS-T, the membranes were incubated at ambient temperature for 1 h with corresponding secondary antibodies. Subsequent to further wash steps, the membrane was treated with the ECL working solution (Solarbio, Beijing, China) and subsequently captured via using imaging techniques (Tanon, Shanghai, China).

The staining of JC-1 and ferrous ions

A group-based treatment procedure was carried out via seeding macrophages in 48-well plates. The JC-1 assay (Beyotime, C2006) was used to estimate mitochondrial membrane potential and iron ion staining was conducted via using ferroOrange (DOJINDO, F374) in view of the manufacturer's protocols.

Hematoxylin–eosin (HE) staining

The HE staining procedure was carried out in view of the manufacturer's instructions for the HE Staining Kit (Solarbio, Beijing, China). Specifically, tissue sections measuring 6 μm in thickness were first stained with hematoxylin for 5 min followed by a 5-min immersion in tap water. Subsequently, the sections were stained with eosin for 10 min, dehydrated with 95% and 100% ethanol, cleared with xylene, and mounted. Microscopic images were captured and analyzed via using Image J software.

Masson staining

Using the Masson's Trichrome Staining Kit (Solarbio, Beijing, China), collagen fibers were analyzed on paraffin sections from Bouin-fixed samples. The collagen content was determined through microscopic observation and analysis with Image-J.

Oil-red staining

To conduct en face Oil Red O (Jiancheng, Nanjing, China) staining of the entire aorta, the aorta is excised

from the heart up to 3–5 mm past the iliac bifurcation. Following removal of external adipose tissue and connective structures, the aorta is longitudinally opened and subjected to Oil Red O staining for a duration of 15 min. Subsequently, the Oil Red O dye is removed via using 70% ethanol, followed by rinsing with running water prior to imaging. All images were captured via utilizing an optical microscope equipped with an image analysis system.

Agilent Seahorse XF cell mito stress test assay

The Agilent Seahorse XFe96 analyzer was used to measure the oxygen consumption rate (OCR), basal ventilation, maximal ventilation, and ATP production ventilation. Specifically, 2×10^4 cells/well were plated in a 96-well XF cell culture microplate in 1640 medium 48 h prior to the experiment. A 45-min incubation at 37 °C in an incubator was conducted after replacing 1640 medium with Seahorse medium (pH 7.4). Afterward, oligomycin (1.5 μM), FCCP (2 μM), and Rot/AA (0.5 μM) were sequentially injected into the cells. As for the data analysis, the results were normalized in relation to the cell numbers via using the Seahorse XF Cell Mito Stress Test Report Generator package.

ELISA

The level of serum TNF-α, IL-8 and IL-1β were determined with the corresponding ELISA kits (Bioscience, Wuhan, China).

The level of MDA and activity of SOD

Based on the manufacture's protocols, the level of malondialdehyde (MDA) and the activity of superoxide dismutase (SOD) of artery lysates were quantified via using commercially available kits (#S0131, #S0101 M, Beyotime), which were operated at specific wavelengths of 532 nm and 450 nm, respectively.

The level of GSH

In view of manufacturer's instructions, the GSH levels of artery lysates were determined via using a glutathione assay kit (Jiancheng, Nanjing, China). Specifically, 100 μl of precipitant was added to the different groups, which were then centrifuged at 3500 rpm for 10 min to extract the supernatant. The supernatant was mixed with 125 μl of working solution for 5 min and Microplate readers from Molecular Devices were used to determine the luminescence, which was measured at 405 nm. Using the protein concentration as a reference, GSH concentrations were normalized within each group.

Real-time reverse transcription-PCR

In accordance with the manufacturer's guidelines (Invitrogen, California, USA), trizol was employed for the extraction of total RNA from arteries. Subsequently, the synthesization of cDNA was operated via utilizing the Reverse Transcription kit (Roche, Basel, Switzerland), followed by quantitative polymerase chain reaction (qPCR) analysis via utilizing SYBR Green (Roche, Basel, Switzerland). Normalization of all data was conducted relative to the mRNA expression level of GAPDH.

Statistical analysis

All the results were presented as mean ± standard error of mean, and all the data were acquired from at least three independent experiments. Two-tailed Student's t-test was used to compare data between two groups with normal distributed values. Mann–Whitney U test was used to compare data between two groups with non-normal distributed values. One-way analysis of variance (ANOVA) was performed for multiple comparisons. Statistical analysis was performed by SPSS 21.0 software. $p<0.05$ was considered statistically significant.

Results

Synthesis and characterization of modified ZIF90 NPs

ZIF90 NPs with a consistent morphology were successfully synthesized, as is confirmed by the electron microscopy. The nanoparticles exhibit a uniform particle size and multiple facets. Furthermore, NPs surface modification of polyvinylpyrrolidone (PVP) or drug loading did not alter the morphology significantly (Fig. 1A). The DLS data illustrated that there was no significant difference in the hydrodynamic sizes between nSP and ZIF90 PVP (Fig. 1B, C). XRD was used to analysis the crystalline structure of NPs, the results showed that the CD16/32-ZIF90@Sp maintained the same crystalline structure as the unmodified ZIF90 PVP NPs (Fig. 1D). The characteristic peak of aldehyde group in 2750 cm^{-1} of ZIF90 was found by infrared spectrum analysis, while aldehyde group characteristic peak disappeared in CD16/32-ZIF90@Sp (Fig. 1E). We further analyzed the stability of CD16/32-ZIF90@Sp in H_2O. The CD16/32-ZIF90@Sp were left in H_2O for 7, 14, 21 and 28 days, respectively, it could be observed that the NPs were essentially constant in size and well dispersed. Moreover, the CD16/32-ZIF90@Sp were placed in DMEM medium, PBS and water for 7, 14, 21 and 28 days, respectively, and assayed for nanoparticle size and potential. The results demonstrated that the particle size and polymer dispersion index (PDI) of CD16/32-ZIF90@Sp remained stable across various environments, suggesting good stability (Fig. 1F, Fig. 2A–C). Subsequent evaluation of the pH

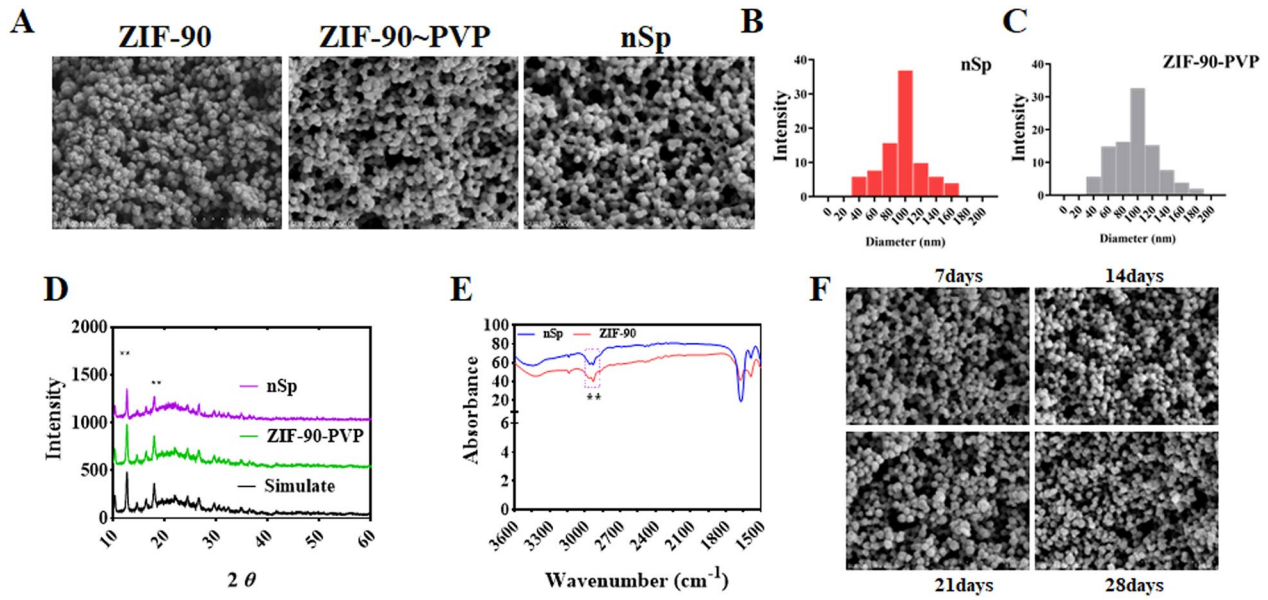

Fig. 1 Characterization of CD16/32-ZIF90@Sp. **A** TEM image of ZIF90, ZIF-PVP and CD16/32-ZIF90@Sp. **B**, **C** Particlesize distribution of ZIF90 and CD16/32-ZIF90@Sp. **D** XRD spectra of ZIF90 and CD16/32-ZIF90@Sp. **E** FTIR spectra of ZIF90 and CD16/32-ZIF90@Sp. **F** TEM images of CD16/32-ZIF90@Sp at 7, 14, 21 and 28 days in water

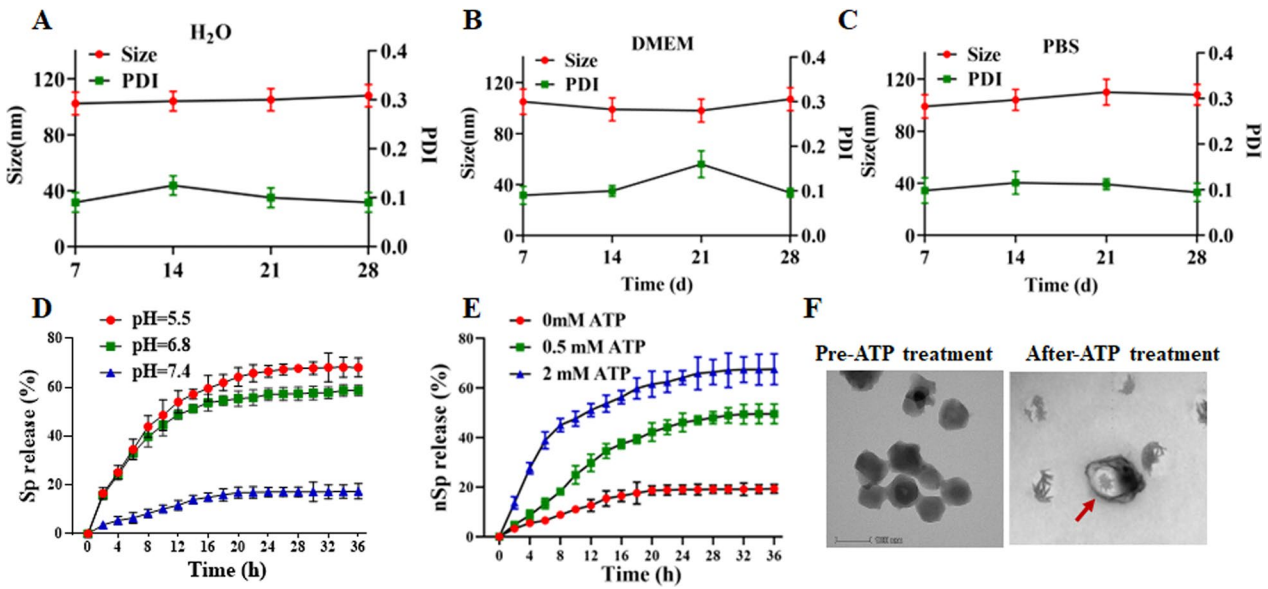

Fig. 2 Stable and drug release of CD16/32-ZIF90@Sp. **A**–**C** Size and PDI index of CD16/32-ZIF90@Sp at 7, 14, 21 and 28 days in H_2O, DMEM and PBS. **D** pH-responsive release curves of CD16/32-ZIF90@Sp. **E** ATP-responsive release curves of CD16/32-ZIF90@Sp. **F** TEM image of ATP-responsive release of CD16/32-ZIF90@Sp

responsiveness of CD16/32-ZIF90@Sp revealed that less than 20% of the drug was released in a pH 7.4 environment, with a notable increase in drug [28] release rate as pH decreased (Fig. 2D). Moreover, the release of CD16/32-ZIF90@Sp was found to be dependent on ATP concentration, as is evidenced by the observation that less than 20% of Sp was released in an ATP-free environment. Nevertheless, as ATP concentration rose, there was a gradual increase in Sp release (Fig. 2E). Furthermore, observation from the electron microscopy revealed that CD16/32-ZIF90@Sp exhibited signs of cracking and collapse in the presence of 2 mM ATP for 12 h (Fig. 2F).

In order to calculate loading capacity and encapsulation efficiency, according to our previous study [28], high performance liquid chromatography (HPLC) was used to detect Sp concentration. We found that the encapsulation efficiency and loading capacity of Sp inCD16/32-ZIF90@Sp were 93.17 ± 1.18% and 30.09 ± 0.20%, respectively.

Targeting ability and cytotoxicity of CD16/32-ZIF90@Sp in vitro

CCK-8 and LDH assay were employed to evaluate the cytotoxicity of CD16/32-ZIF90@Sp on THP-1-derived macrophages. The results from CCK-8 assay demonstrated that a dose-dependent response, with CD16/32-ZIF90@Sp could reduce the cell viability from 98.1% to 58.7% at 24 h, and CD16/32-ZIF90@Sp could reduce the cell viability from 98.9% to 72.1% at doses ranging from 1 to 20 μg/mL (Fig. 3A). Furthermore, after 48 h of treatment, CD16/32-ZIF90@Sp and Sp exhibited more pronounced inhibitory effects on macrophage viabilities (Fig. 3B). The results of LDH were consistent with those of CCK-8, demonstrating that CD16/32 modified ZIF90 could attenuate cytotoxicity of Sp on macrophages (Fig. 3C, D). Subsequent analysis of macrophage damage via using Hoechst-PI staining revealed that CD16/32-ZIF90@Sp administration significantly decreased cytotoxicity compared with 10 μg/mL Sp administration for 24 h (Fig. 3E, F). As a result, a concentration of 5 μg/mL Sp and CD16/32-ZIF90@Sp were selected for further experimentation.

In order to trace the intracellular distribution of NPs, NPs were labeled via using Dil. The results indicated a significant overlap between the Dil signal and mitochondria within the cell. Furthermore, blocking CD16/32 or inhibiting ATP production effectively hindered the entry of NPs into macrophages (Fig. 4A, B). Interestingly, incubation with ox-LDL led to a notable increase in Dil signals in macrophages compared with

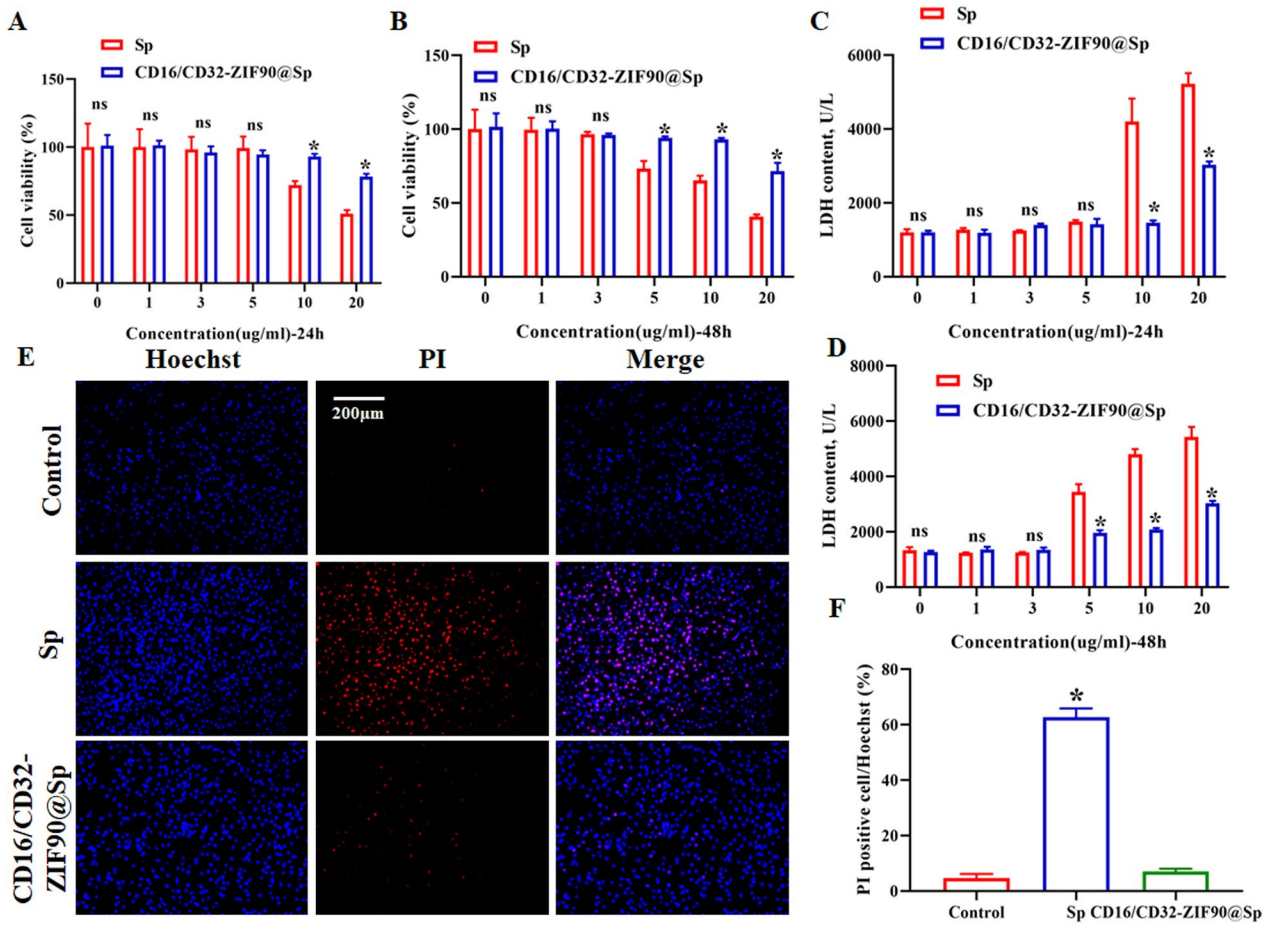

Fig. 3 In vitro cytotoxicity of CD16/32-ZIF90@Sp. **A**, **B** 1, 3, 5, 10 and 20 μg/ml spermine (Sp) and the same quality of Sp in CD16/32-ZIF90@Sp (1.07, 3.22, 5.37, 10.74 and 21.47 μg/ml) was add into the medium for 24 and 48 h. CCK-8 assay was used to detect cell viability, n = 3. *vs Sp, $p < 0.05$. **C**, **D** LDH levels in cell supernatants were assayed, n = 3. * vs Sp, $p < 0.05$. **E**, **F** Hoechst-PI staining was used to detect cell injury, n = 3. *vs control, $p < 0.05$

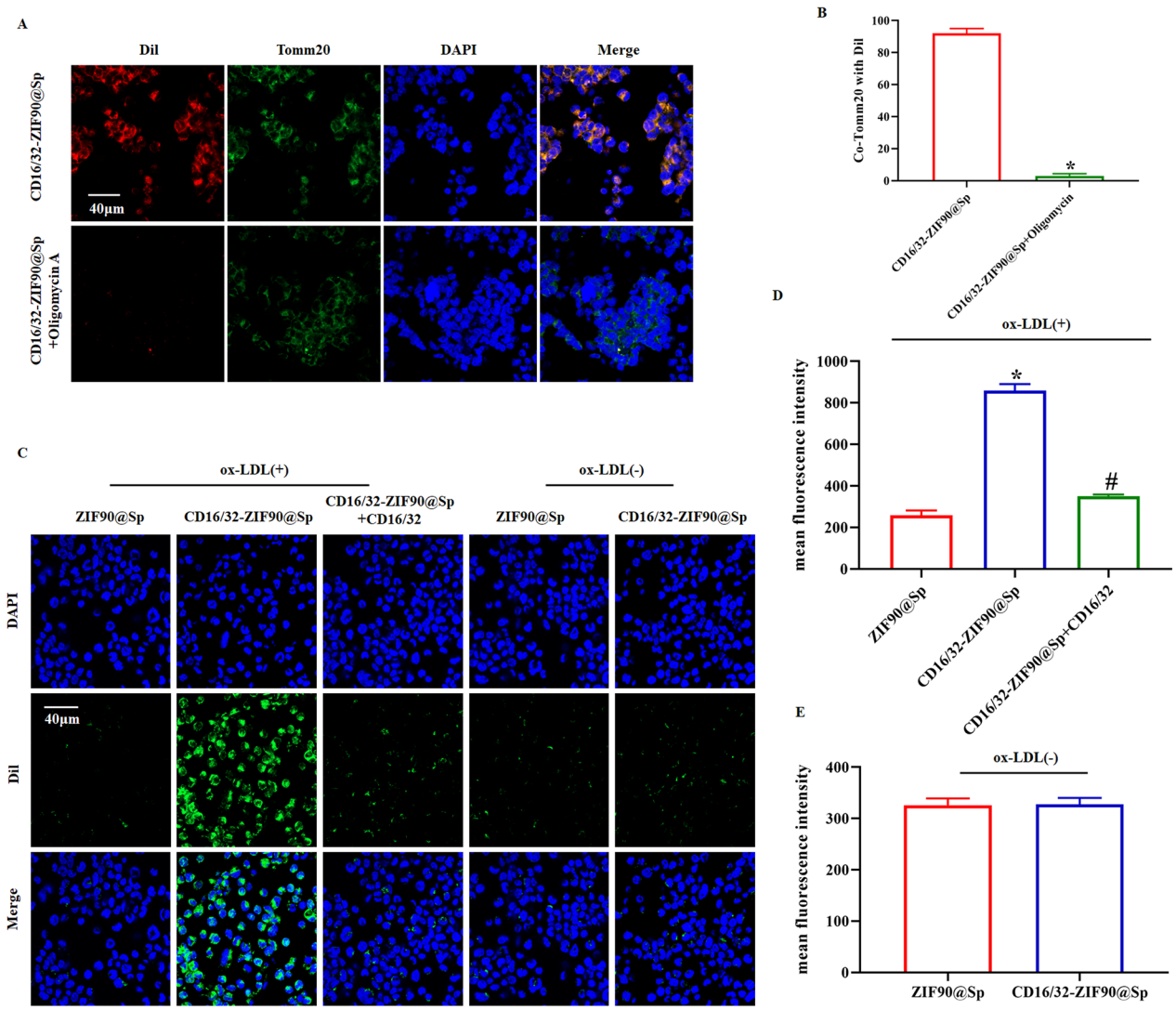

Fig. 4 Localization of CD16/32-ZIF90@Sp in macrophages. **A**, **B** CD16/32-ZIF90@Sp was labeled with Dil. The macrophages were pre-treated with 50 ng/ml oligomycin A for 1 h. Dil and Tomm20 was used to observe co-colocation CD16/32-ZIF90@Sp and mitochondrial. n = 3. *vs CD16/32-ZIF90@Sp, $p < 0.05$. **C**–**E** 100 μg/ml ox-LDL was added into the medium for 24 h; 1 ng/ml CD16/32 antibody was used to block CD16/32. Dil was used to detect the cells absorb the nanoparticles. n = 3. * vs ZIF90@Sp, $p < 0.05$

those not treated with ox-LDL, whose effects were reversed by CD16/32 blocking (Fig. 4C–E).

To further assess the binding efficiency of NPs, macrophages treated with ox-LDL were incubated with CD16/32-ZIF90@Sp or ZIF90@Sp for different time. The results demonstrated that, from 0 to 4 h, the fluorescence intensity of the ZIF90@Sp group exhibited a slight increase, whereas the CD16/32-ZIF90@Sp group showed a rapid increase in the fluorescence intensity (Fig. 5A, B). Moreover, the mechanism by which CD16/32-ZIF90@Sp-entering into macrophages was investigated. According to previous studies, the CD16/32-ZIF90@Sp uptake by cells primarily relies on endocytosis (mediated by clathrin or caveolae), cytosolization and macropinocytosis. In pre-treated cells with inhibitors targeting various pathways, it was observed that nystatin, dynasore, and genistein (clathrin mediated endocytosis inhibitor) could reduce the uptake of NPs, while amiloride (cytosolization and macropinocytosis inhibitor), sucrose (caveolae mediate endocytosis inhibitor) and chlorpromazine (endocytosis) had no impact on the uptake of CD16/32-ZIF90@Sp (Fig. 5C, D). These findings suggested the uptake of CD16/32-ZIF90@Sp by macrophage was dependent on clathrin mediated endocytosis.

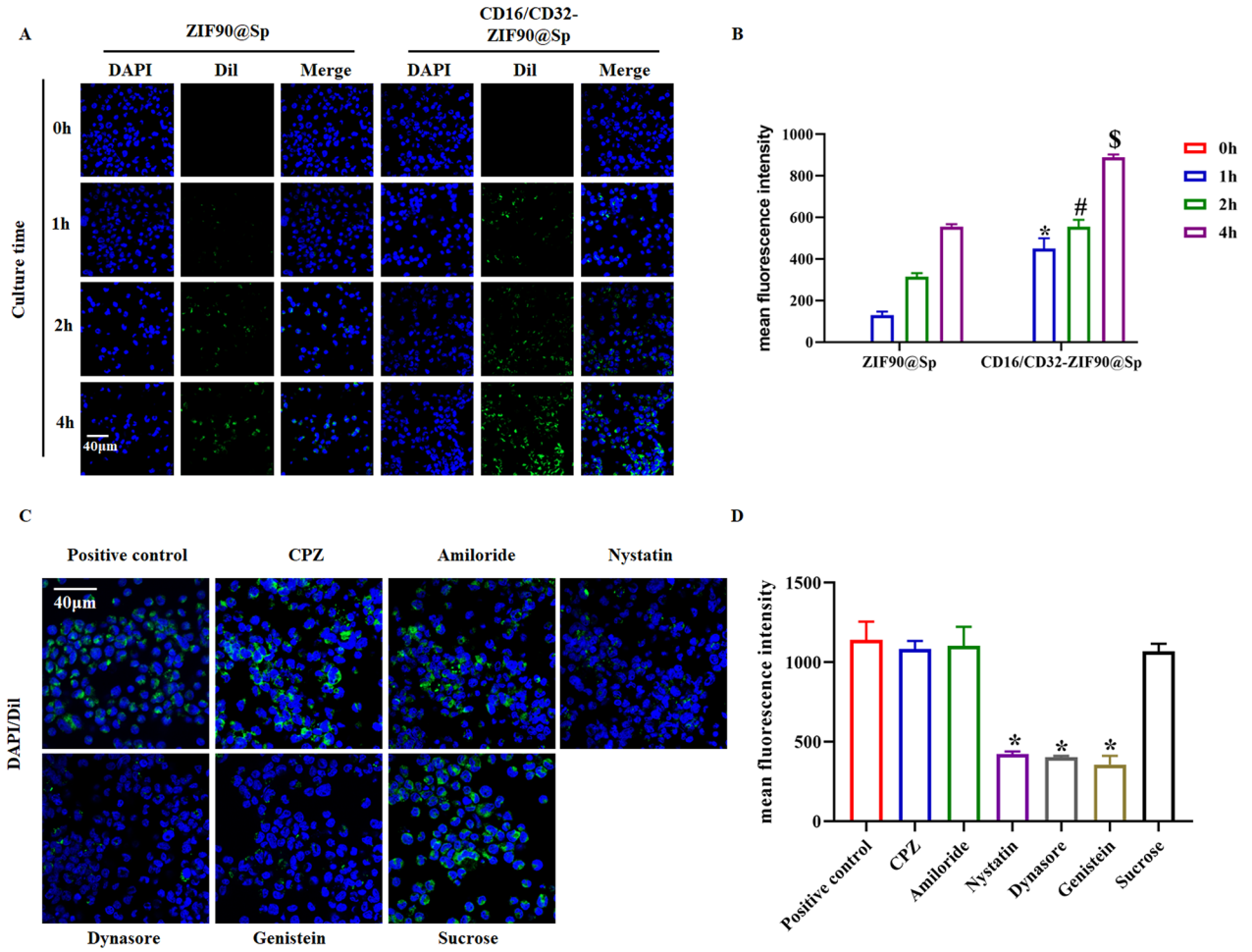

Fig. 5 Targeting ability of CD16/32-ZIF90@Sp in vitro. **A**, **B** CD16/32-ZIF90@Sp and CD16/32-ZIF90@Sp were added into medium from 0-4 h. Observation of fluorescence intensity of Dil in cells. n = 3. * vs 0 h group, $p < 0.05$; # vs 1 h group, $p < 0.05$; $ vs 2 h group, $p < 0.05$. **C**, **D** Macrophages were incubated with fluorescent nanoparticles while the inhibitors chlorpromazine (CPZ,10 g/mL), amiloride hydrochloride (Amiloride,0.1 mM), mycobacterial mycotoxin (Nystatin,10 g/mL), Dynasore (1.6 mM), genistein (100 μg/mL), sucrose (sucrose, 0.45 mM) were tested to monitor the cellular uptake of macrophage uptake nanoparticles. n = 3. * vs positive control, $p < 0.05$

In vivo targeting of atherosclerotic plaques by CD16/32-ZIF90@Sp

In order to investigate the targeting capabilities of CD16/32-ZIF90@Sp towards atherosclerotic lesions and its pharmacokinetics, ApoE$^{-/-}$ mice were intraperitoneal injection with CD16/32-ZIF90@Sp and ZIF90@Sp labeled with Dil, while control group received saline. The results indicated a minimal Dil signal in the arteries of the ZIF90@Sp group compared with the control group, whereas the Dil signal was significantly elevated in the CD16/32-ZIF90@Sp group compared with that in the ZIF90@Sp group (Fig. 6A, B). Also, Dil signal was detected in the liver, kidneys and spleen, with no significant disparity in signal intensity observed between the two experimental groups (Fig. 6C). Furthermore, immunostaining of the aortic roots indicated that Dil signals exhibited reduced strength in the ZIF90@Sp group and displayed less colocalization with macrophages. Conversely, in the CD16/32-ZIF90@Sp group, Dil signals demonstrated a high degree of overlap with macrophages (Fig. 6D). These findings revealed that CD16/32-ZIF90@Sp exhibited a markedly enhanced capacity of binding with macrophage within atherosclerotic plaques compared with ZIF90@Sp.

Evaluation of the therapeutic efficacy and safety of CD16/32-ZIF90@Sp in ApoE$^{-/-}$ mice

Further experimental was performed to analysis the protective effects of CD16/32-ZIF90@Sp administration on AS in ApoE$^{-/-}$ mice fed with high fat diet. The mice were divided into five groups, HE staining was used to evaluate the area of the atherosclerotic plaque in aortic root, it was found that CD16/32-ZIF90 administration had no significant impact on the atherosclerotic plaque

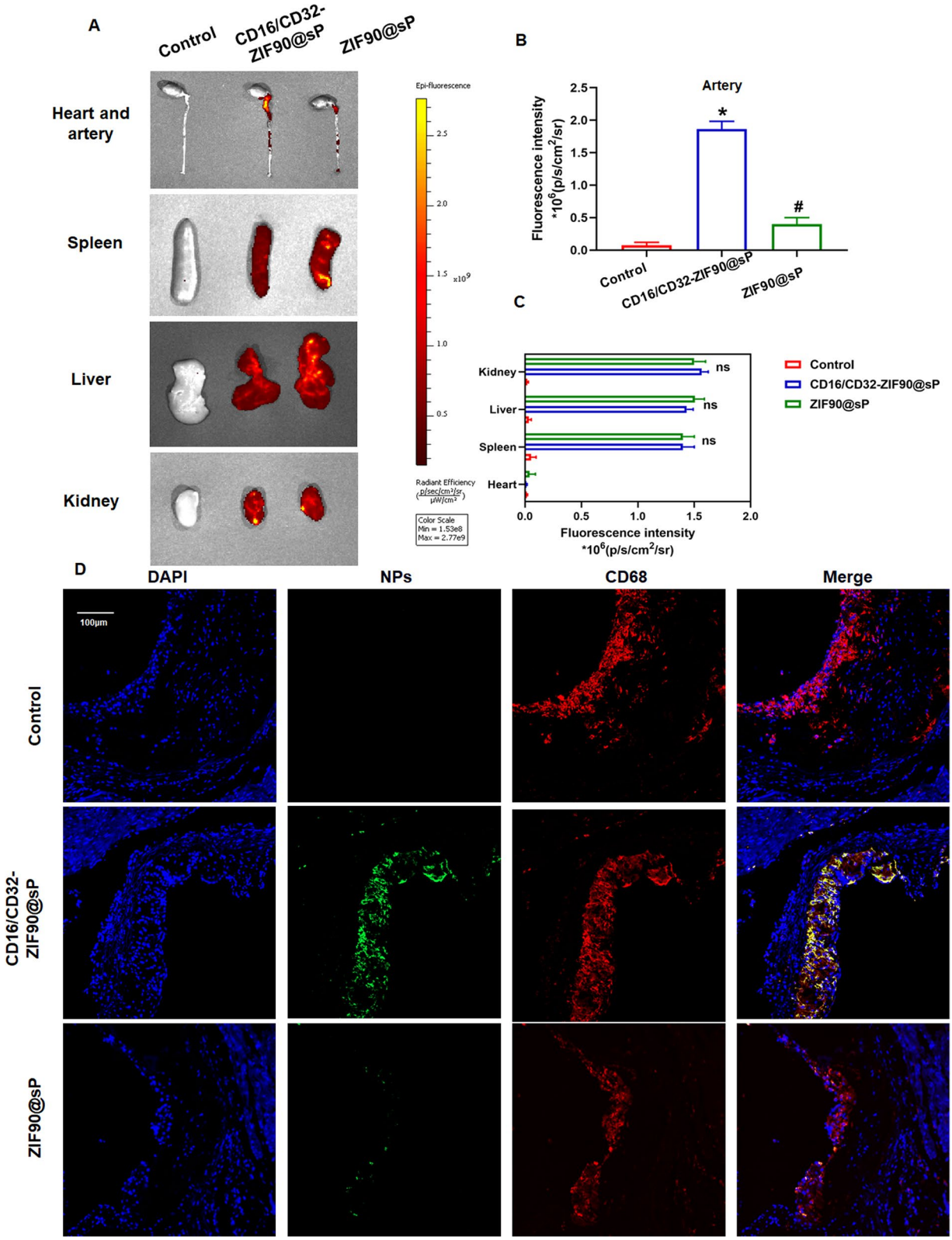

Fig. 6 Targeting atherosclerotic plaques by CD16/32-ZIF90@Sp in vivo. **A** Representative ex vivo fluorescence images of aortas and major Organs. **B** Quantitative data of Dir fluorescent signals accumulated in the aortas. n = 3. **C** Heatmap of Dir fluorescent signals in major organs at 24 h post injection. n = 3. **D** images of aortic sinus sections prepared from atherosclerotic mice after injection of saline, Dir-labeled ZIF90@Sp or CD16/32-ZIF90@Sp for 24 h. n = 3. * vs control group, $p < 0.05$; # vs CD16/32-ZIF90@Sp group, $p < 0.05$

progression in ApoE$^{-/-}$ mice, while Sp administration diminished the plaque area. Furthermore, compared with Sp group, CD16/32-ZIF90@Sp administration further reduced the plaque area (Fig. 7A, C). Collagen fiber deposition suggests increased stability of atherosclerotic plaques, the results of masson staining revealed that CD16/32-ZIF90@Sp further increased the collagen area in the plaque (Fig. 7B, D). The results of oil red staining revealed that CD16/32-ZIF90 had no obvious effect on lipid deposition on arterial surface. Sp and CD16/32-ZIF90@Sp treatment diminished the lipid deposition area, while the decrease of lipid deposition was more obvious in the CD16/32-ZIF90@Sp group (Fig. 7E, F). The death of macrophage within atherosclerotic plaque could release a lot of inflammatory cytokines, circulating inflammatory factors were also detected in different groups. It was found that Sp administration reduced the expression level of TNF-α, IL-1β and IL-8, and the level of TNF-α, IL-1β and IL-8 was lower in CD16/32-ZIF90@Sp group than Sp group (Fig. 7G–I).

We also evaluated the safety of CD16/32-ZIF90@Sp in ApoE$^{-/-}$ mice. The results of HE staining demonstrated that no obvious histological changed in the main organs of mice from five different groups (Fig. 8A). Meanwhile, there were no significant change in body weight, fasting blood-glucose and daily feed intake between those groups (Fig. 8B–D). Leukocyte counts were also examined in different subgroups of mice, the results showed that high-fat feeding increased the number of circulating leukocytes, but there was no significant difference in the other four groups (Fig. 8E). There was no significant difference of serum ALT, AST, BUN and CRE between those groups. Furthermore, CD16/32-ZIF90@Sp had no effect on blood lipid level (Fig. 8E).

Evaluation of the ferroptosis protective of CD16/32-ZIF90@Sp in vivo *and vitro*

To confirm whether CD16/32-ZIF90@Sp improves atherosclerotic lesion severity via inhibiting ferroptosis, the expression level of GPX4 and xCT was detected. It was analyzed that Sp increased the expression of mRNA and protein of GPX4 and xCT, while the effects were more significant in CD16/32-ZIF90@Sp group (Figs. 9A–C, 10A–C). GSH level and SOD activity represented cellular and tissue anti-oxidant capacity. It was observed that Sp administration increased the expression level of GSH and activation of SOD, while CD16/32-ZIF90@Sp administration increase expression level of GSH and SOD activity than Sp administration (Fig. 11A, B).MDA and 4-HNE are the product of lipid peroxidation of cell membranes and therefore also considered as markers of ferroptosis. The MDA

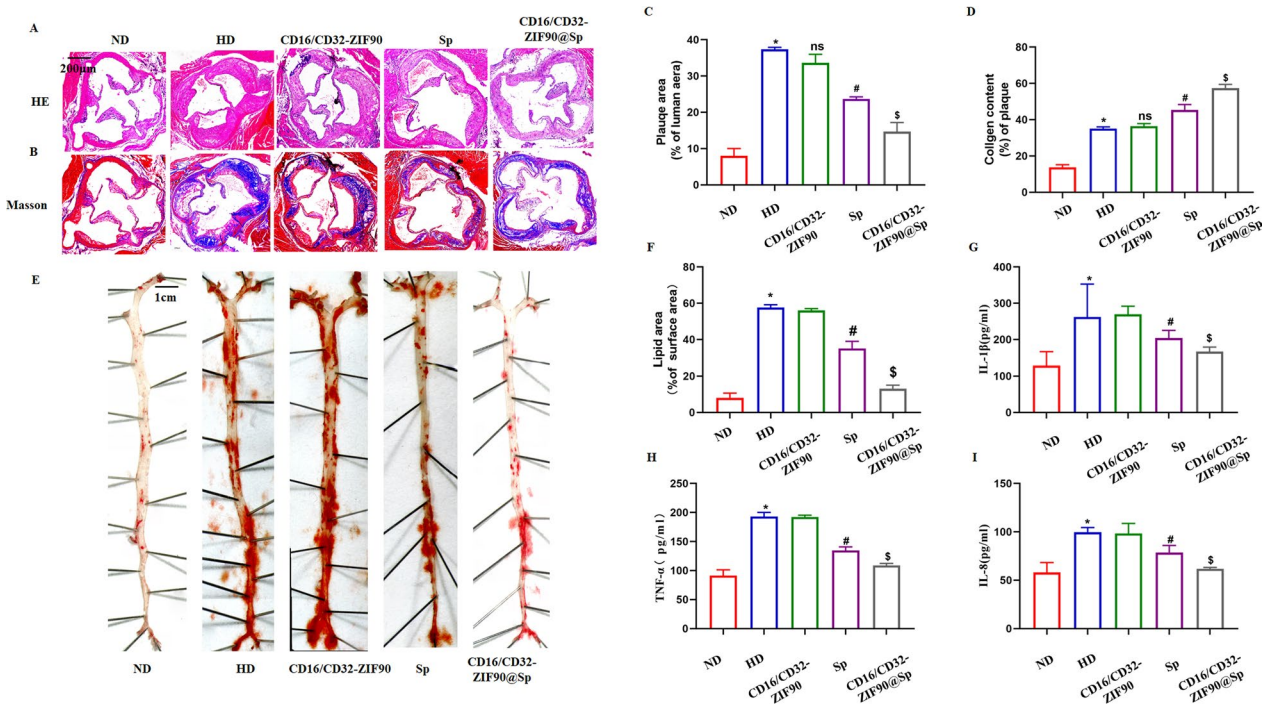

Fig. 7 Assessment of the effect of CD16/32-ZIF90@Sp on the stability of atherosclerotic plaques and measurement of plasma inflammatory cytokines in mice. **A**–**D** HE and Masson staining of the aortic root. n = 3. **E**, **F** Oil red staining of the aortic surface. n = 3. **G**–**I** Serum IL-1β, TNF-α and IL-8 inflammatory factor levels in mice. n = 6. * vs ND group, $p < 0.05$; # vs HD group, $p < 0.05$; $ vs Sp group, $p < 0.05$

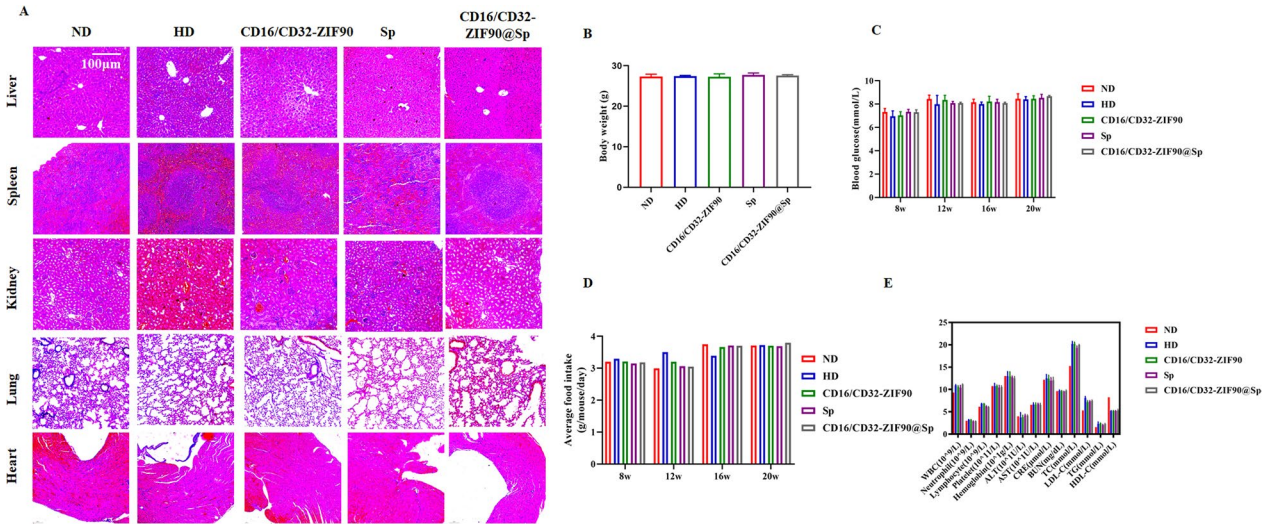

Fig. 8 Biosafety evaluation of CD16/32-ZIF90@Sp in vivo. **A** H&E staining of the heart, liver, spleen, lung, and kidney of ApoE$^{-/-}$ mice after different treatments. **B** Body weight. **C** Fasting blood glucose level. **D** Average food intake. **E** biochemical parameters of ApoE$^{-/-}$ mice after different treatments. n = 6

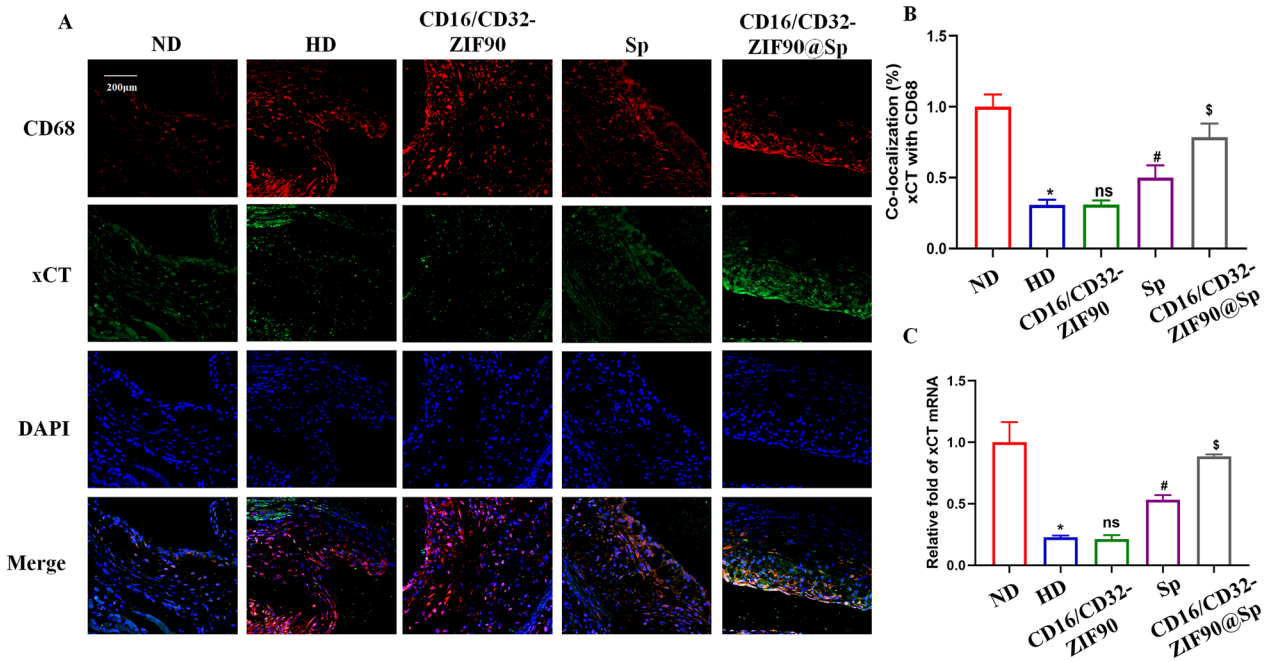

Fig. 9 The effect of CD16/32-ZIF90@Sp on xCT level in ApoE$^{-/-}$ mice. **A**, **B** Co-localization of xCT and CD68 in atherosclerotic plaques. n = 3. **C** xCT mRNA level in aorta. n = 3. * vs ND group, $p < 0.05$; # vs HD group, $p < 0.05$; $ vs Sp group, $p < 0.05$

and 4-HNE in total artery lysate were evaluated, whose results showed that both CD16/32-ZIF90@Sp and Sp administration significantly decreased MDA and 4-HNE, but MDA and 4-HNE were significantly lower in the CD16/32-ZIF90@Sp group than in the Sp group (Fig. 11C, D).

Data in vitro also suggested CD16/32-ZIF90@Sp protected macrophage from ferroptosis. According to our previous studies, ox-LDL could be used to induce ferroptosis of macrophage, The results of CCK-8 and LDH assay demonstrated that CD16/32-ZIF90@Sp and Sp improved cell viability, while the former could improve

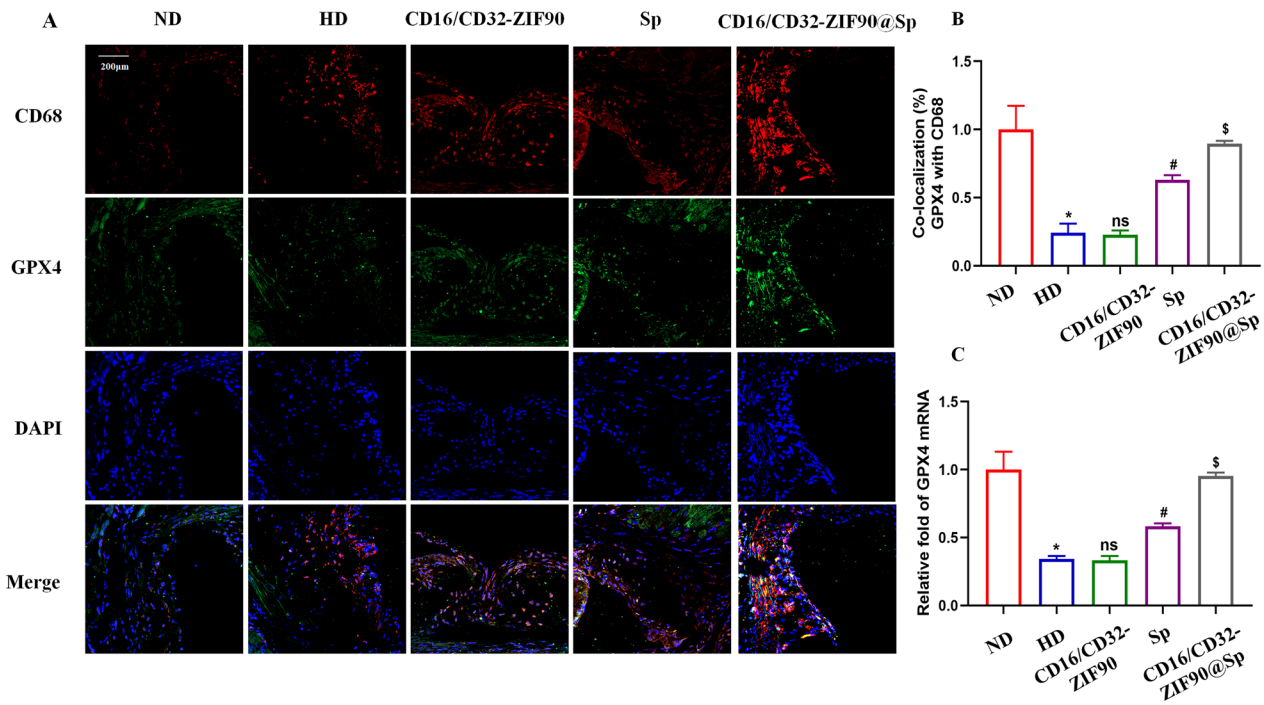

Fig. 10 The effect of CD16/32-ZIF90@Sp on GPX4 level in ApoE$^{-/-}$ mice. **A**, **B** Co-localization of GPX4 and CD68 in AS plaques. n = 3. **C** GPX4 mRNA level in aorta. n = 3. * vs ND group, $p < 0.05$; # vs HD group, $p < 0.05$; $ vs Sp group, $p < 0.05$

more significantly (Fig. 12A, B). Also, the results of FerroOrange staining further demonstrated the inhibitory effect of CD16/32-ZIF90@Sp on ferroptosis of macrophages (Fig. 12D). The results of western blot analysis revealed that CD16/32-ZIF90@Sp increased GPX4 and xCT expression levels in macrophages (Fig. 12E–G). Furthermore, CD16/32-ZIF90@Sp administration decreased the expression level of MDA and 4-HNE in macrophages (Fig. 12H, I). Also, the release of CD16/32-ZIF90@Sp into mitochondria was observed, and the function of macrophage mitochondria was analyzed, whose results indicated that CD16/32-ZIF90@Sp significantly improved mitochondrial membrane potential (Fig. 12C). Furthermore, seahorse test was used to evaluate mitochondrial function, it could be observed that CD16/32-ZIF90@Sp improved mitochondrial respiratory function, whose main manifestations were increased ATP production and maximum respiratory volume (Fig. 12J–L).

Discussion

Anti-platelet and lipid-lowering therapy strategies are the first-line regimens for patients with AS, but several patients still have potential residual cardiovascular risks [2]. Therefore, further investigation is necessary to identify novel therapeutic approaches for AS. In the present study, we reported a metallic nanomaterial targeting atherosclerotic plaque macrophages for delivery of Sp. Our results demonstrated that CD16/32-ZIF90@Sp administration significantly attenuated the progression of atherosclerotic plaque in ApoE$^{-/-}$ mice compared with administrated with Sp alone, as is indicated by reductions in plaque area size and lipid deposition degree as well as an increase in plaque collagen deposition. Furthermore, the study revealed that CD16/32-ZIF90@Sp effectively suppressed the progression of AS by inhibiting macrophage ferroptosis. The results in vivo also confirmed the safety of the nanoparticles. This research offers innovative insights for the development of strategies for the prevention and treatment of AS.

In recent years, metal–organic frameworks have garnered significant interest in biological applications due to their controllable particle diameter and modification capabilities [29, 30]. Among these frameworks, ZIF90 is a common-studied example known for its flexible modifiability and the ability of the aldehyde group on its surface to interact with the amino group of the peptides [31, 32]. Current researches indicate a growing body of evidence confirming the therapeutic effects of ZIF90 as a drug carrier in malignant tumors [33, 34]. There is a study indicating that the delivery of hemin by ZIF90 could enhance the anti-tumor efficacy via targeting degradation of BTB and CNC homology1 [35]. Furthermore, ZIF90 exhibits the mitochondria-target property, releasing the drug upon interacting with ATP within the mitochondria. The

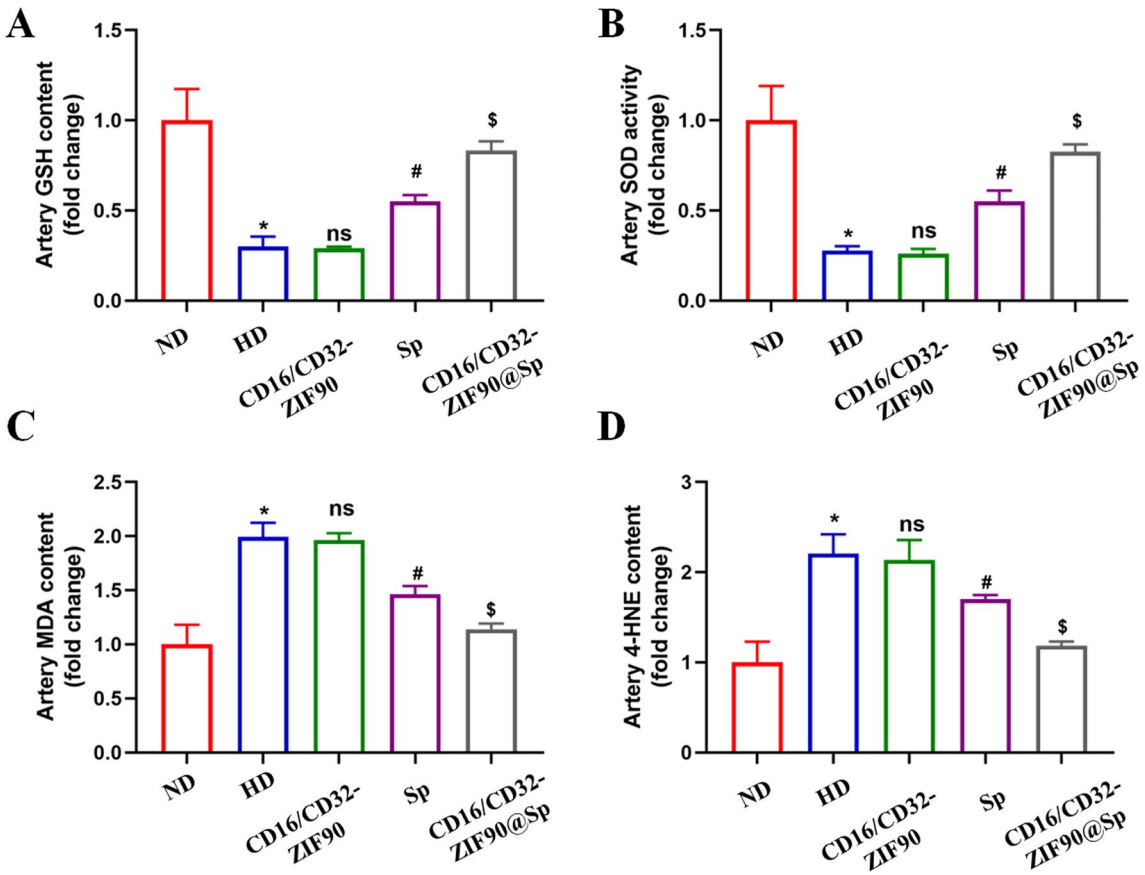

Fig. 11 The effect of CD16/32-ZIF90@Sp on macrophage ferroptpsis in ApoE$^{-/-}$ mice. **A** Aortic GSH levels. n = 3. **B** Aortic SOD activity. n = 3. **C** Aortic MDA levels. n = 3. **D** Aortic 4-HNE activity. n = 3. * vs ND group, $p < 0.05$; # vs HD group, $p < 0.05$; $ vs Sp group, $p < 0.05$

investigation also indicated that ZIF90-meidated drugs release in close to mitochondria significantly enhanced mitochondrial respiration [35]. Another study highlighted the efficacy of ZIF90 in delivering berberine for glioma treatment [36]. AS is considered as a chronic inflammatory vascular disease, ameliorating mitochondrial dysfunction has been identified as the potential therapeutic approach for AS. However, the feasibility of utilizing ZIF90 as a drug carrier to enhance atherosclerotic treatment efficacy and safety remains uncertain.

Prior research has indicated that the use of N'N-dimethylformamide (DMF) as a solvent in the preparation of ZIF90 nanoparticles could lead to the presence of toxic DMF residue [22]. In the current study, a system consisting of tert-butanol, glycerol, water, and PVP was employed for the preparation of ZIF90 nanoparticles. In our investigation, it was noted that the synthesized ZIF90 exhibited improved dispersion, uniform particle sizes and minimal alteration in particle size attributed to the presence of PVP and Sp. The results of XDG and electron microscopy indicated the successful preparation of ZIF90 nanoparticles with consistent particle size and dispersion. Additionally, the results of CCK-8 and LDH assay revealed that ZIF90 NPs mitigated the cytotoxic effects of Sp on cells. This observation aligns with findings reported in literature [37]. Additionally, a previous study has indicated ZIF90 is sensitive to ATP. In ZIF90, zinc ions form coordination bonds with nitrogen atoms of 2-imidazolaldehyde, while ATP can competitively bind single nitrogen atoms with zinc ions. This is the main mechanism that causes ZIF90 to degrade after encountering ATP [38, 39]. The current investigation conducted in vitro experiments revealed that the presence of ATP triggerd the splitting of ZIF90 NPs and the release of drug subsequently. Moreover, it was also observed that the signal of ZIF90 closely aligned with that of the mitochondria. However, the inhibition of mitochondrial ATP synthesis hindered the entry of ZIF90 NPs into macrophages. These findings substantiated the notion that the majority of the drug payload delivered by ZIF90 was released in close proximity to the mitochondria. Furthermore, our results demonstrated that CD16/32-ZIF90@Sp effectively ameliorated the decline in the membrane

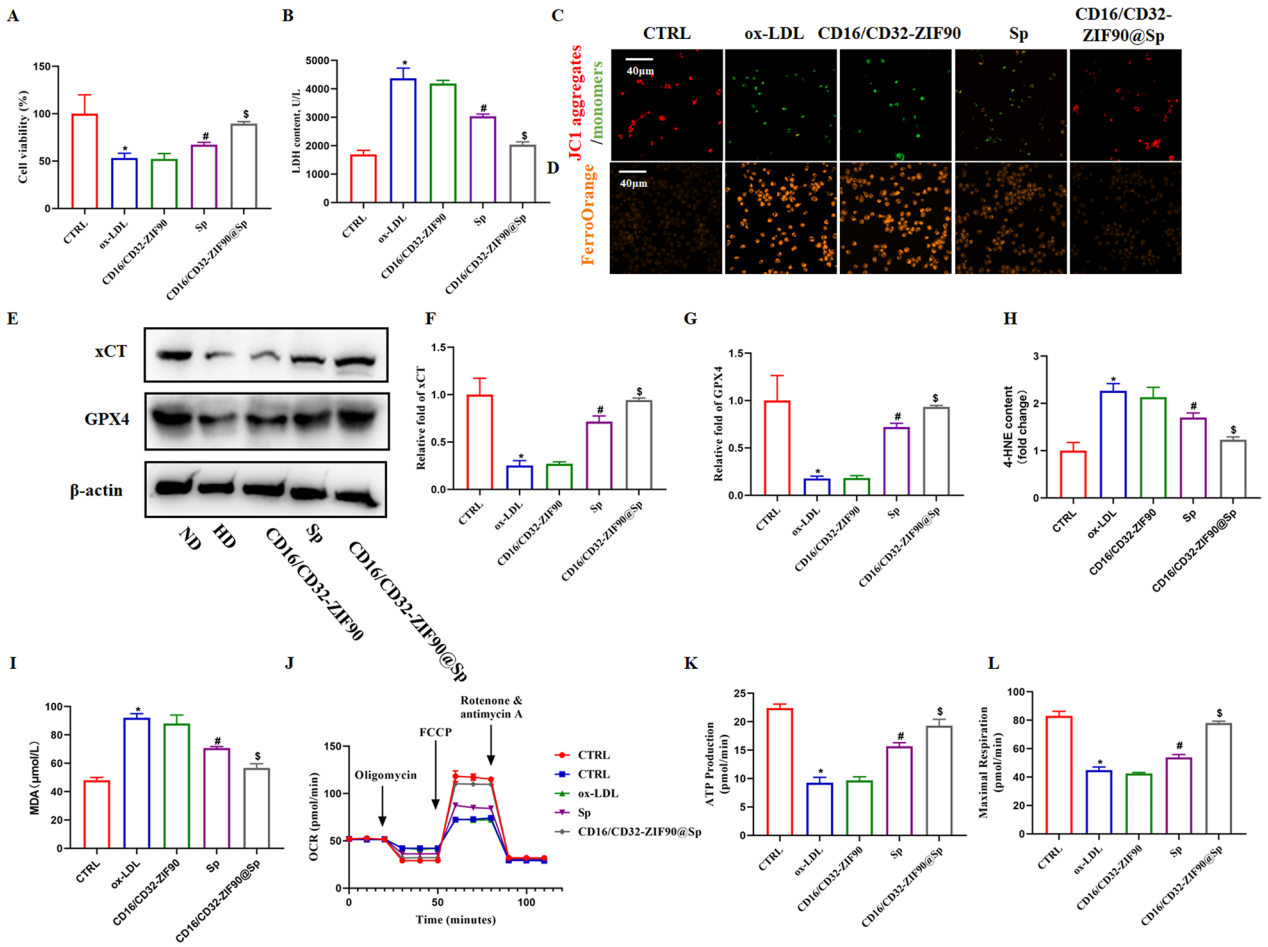

Fig. 12 Inhibitory effect of CD16/32-ZIF90@Sp on macrophage ferroptosis in vitro. 5μ/ml Sp, ZIF90@Sp and CD16/32-ZIF90@Sp added into the medium for 1 h, followed by 100 μg/ml ox-LDL stimulated for 48 h. **A** CCK-8 assay. n = 3. **B** LDH assay. n = 3. **C**, **D** JC-1 and ferroorange staining. n = 3. **E**–**G** Western blot for GPX4 and xCT. n = 3. **H** 4-HNE level. n = 3. (I) MDA level. n = 3. **G** ECAR of macrophages. n = 5. **H** ATP production. n = 5. **I** Maximum respiratory output. n = 5. * vs CTRL group, $p < 0.05$; # vs ox-LDL group, $p < 0.05$; $ vs Sp group, $p < 0.05$

potential and mitochondrial respiratory dysfunction induced by ox-LDL treatment.

In recent years, the study of nanoparticle-delivered drugs to improve macrophage inflammatory response to inhibit the progression of AS has received much attention. However, how to target macrophages for drug delivery is still considered as a challenge. It has been reported that binding the macrophage surface CD44 receptor enabled macrophage-targeted drug delivery [40]. However, both smooth muscle cells and endothelial cells within atherosclerotic plaques also express CD44 receptor, indicated the reduced specificity. Although macrophage membrane-encapsulated biomimetic nanoparticles have shown promise in efficiently targeting macrophages with precision, translating this success to clinical applications remains challenging. [41–43]. CD16/32 serves as a marker for activated macrophages within atherosclerotic plaques, and CD16/32-positive macrophages exhibit heightened inflammatory response, impaired phagocytic function, and increased propensity for apoptosis. Consequently, CD16/32 has been employed as a diagnostic marker for identifying activated macrophages. Previous studies have utilized CD16/32 antibody-modified ZIF8 to inhibit macrophage polarization in mice with arthritis [37]. In the present study, infrared spectroscopy revealed that the CD16/32 antibody modified ZIF90 by aldehyde binding. We found that CD16/32-ZIF90@Sp was almost unable to enter the cells via using CD16/32 antibody, suggesting that CD16/32-ZIF90@Sp enters cells via CD16/32. Furthermore, we also found ZIF90 NPs uptake via clathrin mediated endocytosis after binding to CD16/32. It was also observed in ApoE$^{-/-}$ mice that the CD16/32-ZIF90@Sp signal overlapped almost completely with the macrophage signal within the atherosclerotic plaques, whereas the fluorescent

signal of unmodified CD16/32 NPs was dispersed in the atherosclerotic plaques. These results all suggested that CD16/32-modified ZIF90 could effectively recognize macrophages within atherosclerotic plaques. Ferroptosis, a newly discovered mode of programmed cell death, there is growing evidence that ferroptosis plays an important role in the progression of AS. We previously found that exogenous inhibition of macrophage ferroptosis suppressed atherosclerotic progression in $ApoE^{-/-}$ mice [25]. Other studies have also reported the similar findings [44, 45]. However, to date, no studies have reported that NPs-delivered drugs inhibited the progression of AS by inhibiting macrophage ferroptosis. Our study showed that both CD16/32-ZIF90@Sp and Sp effectively inhibited macrophage ferroptosis, leading to the improved atherosclerotic lesion severity. However, both in vivo and in vitro evidence indicated that CD16/32-ZIF90@Sp had the superior ability to ameliorate the progression of AS and inhibited macrophage ferroptosis more significantly compared with Sp alone. Previous research has also shown that nanomaterial-delivered drugs could impede the development of AS via enhancing macrophage lipid metabolism, polarization, and inflammatory responses [46, 47]. This study contributes novel insights into the mechanisms through which nanoparticle-delivered drugs improve the advancement of AS.

The findings from HE staining indicated that CD16/32-ZIF90@Sp did not exhibit any notable histological changes in the heart, liver, kidney, lungs and spleen. Additionally, the results of hematological assessments also indicated that CD16/32-ZIF90@Sp did not have a significant impact on blood cell counts, liver function and kidney function. Furthermore, lipid levels were not affected by CD16/32-ZIF90@Sp. Taken together, these results suggested the safety profile of CD16/32-ZIF90@Sp in vivo setting.

Conclusion

Our study demonstrated that CD16/32-modified ZIF90 nanoparticles effectively targeted macrophages within atherosclerotic plaques, CD16/32-ZIF90@Sp could inhibit the progression of AS. This effect was attributed to the enhancement of mitochondrial function and inhibition of macrophage ferroptosis with minimal adverse effects. The delivery of Sp via CD16/32-modified ZIF90 nanoparticles showed promise as a potential therapeutic strategy for individuals with AS.

Supplementary Information

The online version contains supplementary material available at https://doi.org/10.1186/s12951-025-03271-8.

Supplementary Material 1.

Acknowledgements
We sincerely thank Mr. Haoran Wang for his assistance in language editing and manuscript writing.

Author contributions
X. L., Y. W..: Acquisition and drafting the work. Y. C., B. X., Q. L, and X. Z.: Acquisition of data for the work, Y. C., B. X., and Y. L. and X. B.: Analysis and interpretation of data, X. L., Y. C., X. W., J. D. and M. L.: Drafting the article. C.X., J.M., M.W., Y. Z., Y. W., X. L. and Y. C.: Revised the manuscript. X. L.: Acquisition. All the authors approved the final manuscript.

Funding
This work was supported by Postdoctoral project in Heilongjiang Province (LBH-Z24219), National Natural Science Foundation of China(82200454), Graduate research and practice innovation project of Harbin Medical University(YJSCX2024-38HYD) and Fund of Key Laboratory of Myocardial Ischemia, Ministry of Education (KF202313, KF202308, KF202410).

Availability of data and materials
No datasets were generated or analysed during the current study.

Declarations

Consent for publication
Yes.

Competing interests
The authors declare that they have no competing interests.

Author details
[1]Department of Cardiology, 2, Affiliated Hospital of Harbin Medical University, Harbin 150001, People's Republic of China. [2]National Key Laboratory of Frigid Zone Cardiovascular Diseases, The Key Laboratory of Myocardial Ischemia, Chinese Ministry of Education, Harbin 150001, People's Republic of China. [3]Department of Thoracic Radiotherapy, Harbin Medical University Cancer Hospital, Harbin 150001, China. [4]Department of Pathophysiology, Harbin Medical University, Harbin 150001, China.

Received: 25 August 2024 Accepted: 24 February 2025
Published online: 04 March 2025

References

1. Libby P. The changing landscape of atherosclerosis. Nature. 2021;592(7855):524–33.
2. Libby P, Bornfeldt KE, Tall AR. Atherosclerosis: successes, surprises, and future challenges. Circ Res. 2016;118(4):531–4.
3. MacRae CA, Califf RM. Reimagining what we measure in atherosclerosis-a "Phenotype Stack." Circ Res. 2020;126(9):1146–58.
4. Riccardi G, Giosuè A, Calabrese I, Vaccaro O. Dietary recommendations for prevention of atherosclerosis. Cardiovasc Res. 2022;118(5):1188–204.
5. Yang S, Yuan HQ, Hao YM, Ren Z, Qu SL, Liu LS, Wei DH, Tang ZH, Zhang JF, Jiang ZS. Macrophage polarization in atherosclerosis. Clin Chim Acta. 2020;501:142–6.
6. Chen W, Schilperoort M, Cao Y, Shi J, Tabas I, Tao W. Macrophage-targeted nanomedicine for the diagnosis and treatment of atherosclerosis. Nat Rev Cardiol. 2022;19(4):228–49.
7. Xie Z, Wang X, Liu X, Du H, Sun C, Shao X, Tian J, Gu X, Wang H, Tian J, et al. Adipose-derived exosomes exert proatherogenic effects by regulating macrophage foam cell formation and polarization. J Am Heart Assoc. 2018. https://doi.org/10.1161/JAHA.117.007442.

8. Jiang X, Stockwell BR, Conrad M. Ferroptosis: mechanisms, biology and role in disease. Nat Rev Mol Cell Biol. 2021;22(4):266–82.
9. Li J, Cao F, Yin HL, Huang ZJ, Lin ZT, Mao N, Sun B, Wang G. Ferroptosis: past, present and future. Cell Death Dis. 2020;11(2):88.
10. Ouyang S, You J, Zhi C, Li P, Lin X, Tan X, Ma W, Li L, Xie W. Ferroptosis: the potential value target in atherosclerosis. Cell Death Dis. 2021;12(8):782.
11. Bai T, Li M, Liu Y, Qiao Z, Wang Z. Inhibition of ferroptosis alleviates atherosclerosis through attenuating lipid peroxidation and endothelial dysfunction in mouse aortic endothelial cell. Free Radic Biol Med. 2020;160:92–102.
12. Tse RT, Wong CY, Chiu PK, Ng CF. The potential role of spermine and its acetylated derivative in human malignancies. Int J Mol Sci. 2022;23(3):1258.
13. Wang Y, Wang Y, Li F, Zhang X, Li H, Yang G, Xu C, Wei C. Spermine protects cardiomyocytes from high glucose-induced energy disturbance by targeting the CaSR-gp78-ubiquitin proteasome system. Cardiovasc Drugs Ther. 2021;35(1):73–85.
14. Wei C, Li HZ, Wang YH, Peng X, Shao HJ, Li HX, Bai SZ, Lu XX, Wu LY, Wang R, et al. Exogenous spermine inhibits the proliferation of human pulmonary artery smooth muscle cells caused by chemically-induced hypoxia via the suppression of the ERK1/2- and PI3K/AKT-associated pathways. Int J Mol Med. 2016;37(1):39–46.
15. Holbert CE, Cullen MT, Casero RA Jr, Stewart TM. Polyamines in cancer: integrating organismal metabolism and antitumour immunity. Nat Rev Cancer. 2022;22(8):467–80.
16. Peng Q, Wong CY, Cheuk IW, Teoh JY, Chiu PK, Ng CF. The emerging clinical role of spermine in prostate cancer. Int J Mol Sci. 2021;22(9):4382.
17. Luo D, Lu X, Li H, Li Y, Wang Y, Jiang S, Li G, Xu Y, Wu K, Dou X, et al. The spermine oxidase/spermine axis coordinates ATG5-mediated autophagy to orchestrate renal senescence and fibrosis. Adv Sci (Weinh). 2024;11:e2306912.
18. Talev J, Kanwar JR. Iron oxide nanoparticles as imaging and therapeutic agents for atherosclerosis. Semin Thromb Hemost. 2020;46(5):553–62.
19. Wang S, He H, Mao Y, Zhang Y, Gu N. Advances in atherosclerosis theranostics harnessing iron oxide-based nanoparticles. Adv Sci (Weinh). 2024;11(17): e2308298.
20. Gao C, Huang Q, Liu C, Kwong CHT, Yue L, Wan JB, Lee SMY, Wang R. Treatment of atherosclerosis by macrophage-biomimetic nanoparticles via targeted pharmacotherapy and sequestration of proinflammatory cytokines. Nat Commun. 2020;11(1):2622.
21. Wang Y, Zhang K, Li T, Maruf A, Qin X, Luo L, Zhong Y, Qiu J, McGinty S, Pontrelli G, et al. Macrophage membrane functionalized biomimetic nanoparticles for targeted anti-atherosclerosis applications. Theranostics. 2021;11(1):164–80.
22. Jiang Z, Yuan B, Qiu N, Wang Y, Sun L, Wei Z, Li Y, Zheng J, Jin Y, Li Y, et al. Manganese-zeolitic imidazolate frameworks-90 with high blood circulation stability for MRI-guided tumor therapy. Nanomicro Lett. 2019;11(1):61.
23. Chen J, Bao Y, Song Y, Zhang C, Qiu F, Sun Y, Xin L, Cao J, Jiang Y, Luo J, et al. Hypoxia-alleviated nanoplatform to enhance chemosensitivity and sonodynamic effect in pancreatic cancer. Cancer Lett. 2021;520:100–8.
24. Jiang Z, Wang Y, Sun L, Yuan B, Tian Y, Xiang L, Li Y, Li Y, Li J, Wu A. Dual ATP and pH responsive ZIF-90 nanosystem with favorable biocompatibility and facile post-modification improves therapeutic outcomes of triple negative breast cancer in vivo. Biomaterials. 2019;197:41–50.
25. Luo X, Wang Y, Zhu X, Chen Y, Xu B, Bai X, Weng X, Xu J, Tao Y, Yang D, et al. MCL attenuates atherosclerosis by suppressing macrophage ferroptosis via targeting KEAP1/NRF2 interaction. Redox Biol. 2024;69: 102987.
26. Luo X, Weng X, Bao X, Bai X, Lv Y, Zhang S, Chen Y, Zhao C, Zeng M, Huang J, et al. A novel anti-atherosclerotic mechanism of quercetin: competitive binding to KEAP1 via Arg483 to inhibit macrophage pyroptosis. Redox Biol. 2022;57: 102511.
27. Mahmood T, Yang PC. Western blot: technique, theory, and trouble shooting. N Am J Med Sci. 2012;4(9):429–34.
28. Wei C, Li H, Wang Y, Peng X, Shao H, Li H, Bai S, Xu C. Exogenous spermine inhibits hypoxia/ischemia-induced myocardial apoptosis via regulation of mitochondrial permeability transition pore and associated pathways. Exp Biol Med (Maywood). 2016;241(14):1505–15.
29. Cun JE, Fan X, Pan Q, Gao W, Luo K, He B, Pu Y. Copper-based metal-organic frameworks for biomedical applications. Adv Colloid Interface Sci. 2022;305: 102686.
30. Chen J, Zhu Y, Kaskel S. Porphyrin-based metal-organic frameworks for biomedical applications. Angew Chem Int Ed Engl. 2021;60(10):5010–35.
31. Cai M, Yao Y, Yin D, Zhu R, Fu T, Kong J, Wang K, Liu J, Yao A, Ruan Y, et al. Enhanced lysosomal escape of cell penetrating peptide-functionalized metal-organic frameworks for co-delivery of survivin siRNA and oridonin. J Colloid Interface Sci. 2023;646:370–80.
32. Huang X, Lin D, Duan P, Chen H, Zhao Y, Yang W, Pan Q, Tian X. Space-confined growth of nanoscale metal-organic frameworks/Pd in hollow mesoporous silica for highly efficient catalytic reduction of 4-nitrophenol. J Colloid Interface Sci. 2023;629(Pt B):55–64.
33. Yu M, Zeng W, Ouyang Y, Liang S, Yi Y, Hao H, Yu J, Liu Y, Nie Y, Wang T, et al. ATP-exhausted nanocomplexes for intratumoral metabolic intervention and photoimmunotherapy. Biomaterials. 2022;284: 121503.
34. Zhao X, Wang Y, Jiang W, Wang Q, Li J, Wen Z, Li A, Zhang K, Zhang Z, Shi J, et al. Herpesvirus-mimicking DNAzyme-loaded nanoparticles as a mitochondrial DNA stress inducer to activate innate immunity for tumor therapy. Adv Mater. 2022;34(37): e2204585.
35. Lu L, Liu G, Lin C, Li K, He T, Zhang J, Luo Z, Cai K. Mitochondrial metabolism targeted nanoplatform for efficient triple-negative breast cancer combination therapy. Adv Healthc Mater. 2021;10(20): e2100978.
36. Monarca L, Ragonese F, Sabbatini P, Caglioti C, Stamegna M, Palazzetti F, Sportoletti P, Costantino F, Fioretti B. Synthesis and characterization of ZIF-90 nanoparticles as potential brain cancer therapy. Pharmaceutics. 2024;16(3):414.
37. Zhou F, Mei J, Yang S, Han X, Li H, Yu Z, Qiao H, Tang T. Modified ZIF-8 Nanoparticles Attenuate Osteoarthritis by Reprogramming the Metabolic Pathway of Synovial Macrophages. ACS Appl Mater Interfaces. 2020;12(2):2009–22.
38. Pan W, Cui B, Wang K, Shi M, Lu F, Li N, Tang B. ATP-triggered mitochondrial cascade reactions for cancer therapy with nanoscale zeolitic imidazole framework-90. Theranostics. 2021;11(16):7869–78.
39. Deng XC, Liang JL, Zhang SM, Wang YZ, Lin YT, Meng R, Wang JW, Feng J, Chen WH, Zhang XZ. Interference of ATP-adenosine axis by engineered biohybrid for amplifying immunogenic cell death-mediated antitumor immunotherapy. Adv Mater (Deerfield Beach, Fla). 2024;36(36): e2405673.
40. Yu J, Ma Y, Zhang X, Wang S, Zhou L, Liu X, Li L, Liu L, Song H, Luo Y, et al. β-cyclodextrin and hyaluronic acid-modified targeted nanodelivery system for atherosclerosis prevention. ACS Appl Mater Interfaces. 2024;16(27):35421–37.
41. Zhu L, Zhong Y, Yan M, Ni S, Zhao X, Wu S, Wang G, Zhang K, Chi Q, Qin X, et al. Macrophage membrane-encapsulated dopamine-modified poly cyclodextrin multifunctional biomimetic nanoparticles for atherosclerosis therapy. ACS Appl Mater Interfaces. 2024;16(25):32027–44.
42. He Z, Chen Q, Duan X, Zhong Y, Zhu L, Mou N, Yang X, Cao Y, Han Z, He H, et al. Reactive oxygen species-responsive nano-platform with dual-targeting and fluorescent lipid-specific imaging capabilities for the management of atherosclerotic plaques. Acta Biomater. 2024;181:375–90.
43. Nankivell V, Vidanapathirana AK, Hoogendoorn A, Tan JTM, Verjans J, Psaltis PJ, Hutchinson MR, Gibson BC, Lu Y, Goldys E, et al. Targeting macrophages with multifunctional nanoparticles to detect and prevent atherosclerotic cardiovascular disease. Cardiovasc Res. 2024;120(8):819–38.
44. Hong Y, Feng J, Dou Z, Sun X, Hu Y, Chen Z, Liu L, Xu H, Du M, Tang P, et al. Berberine as a novel ACSL4 inhibitor to suppress endothelial ferroptosis and atherosclerosis. Biomed Pharmacother. 2024;177: 117081.
45. Tao Y, Zhao Q, Lu C, Yong W, Xu M, Wang Z, Leng X. Melatonin suppresses atherosclerosis by ferroptosis inhibition via activating NRF2 pathway. Faseb j. 2024;38(10): e23678.
46. Zhen J, Li X, Yu H, Du B. High-density lipoprotein mimetic nano-therapeutics targeting monocytes and macrophages for improved cardiovascular care: a comprehensive review. J Nanobiotechnology. 2024;22(1):263.
47. Qiu S, Liu J, Chen J, Li Y, Bu T, Li Z, Zhang L, Sun W, Zhou T, Hu W, et al. Targeted delivery of MerTK protein via cell membrane engineered nanoparticle enhances efferocytosis and attenuates atherosclerosis in diabetic ApoE(-/-) Mice. J Nanobiotechnology. 2024;22(1):178.

Publisher's Note